Chapter 5
High Efficiency Multijunction Solar Cells with Finely-Tuned Quantum Wells

Argyrios C. Varonides

The field of high efficiency (inorganic) photovoltaics (PV) is rapidly maturing in both efficiency goals and cover all cost reduction of fabrication. On one hand, know-how from space industry in new solar cell design configurations and on the other, fabrication cost reduction challenges for terrestrial uses of solar energy, have paved the way to a new generation of PV devices, capable of capturing most of the solar spectrum. For quite a while now, the goal of inorganic solar cell design has been the total (if possible) capture-absorption of the solar spectrum from a single solar cell, designed in such a way that a multiple of incident wavelengths could be simultaneously absorbed. Multi-absorption in device physics indicates parallel existence of different materials that absorb solar photons of different energies. Bulk solid state devices absorb at specific energy thresholds, depending on their respective energy gap (E_G). More than one energy gaps would on principle offer new ways of photon absorption: if such a structure could be fabricated, two or more groups of photons could be absorbed simultaneously. The point became then what lattice-matched semiconductor materials could offer such multiple levels of absorption without much recombination losses. It was soon realized that such layer multiplicity combined with quantum size effects could lead to higher efficiency collection of photo-excited carriers. At the moment, the main reason that slows down quantum effect solar cell production is high fabrication cost, since it involves primarily expensive methods of multilayer growth. Existing multi-layer cells are fabricated in the bulk, with three (mostly) layers of lattice-matched and non-lattice-matched (pseudo-morphic) semiconductor materials (GaInP/InGaN etc), where photo-carrier collection occurs in the bulk of the base (coming from the emitter which lies right under the window layer). These carriers are given excess to conduction via tunnel junction (grown between at each interface and connecting the layers in series). This basic idea of a design has proven very successful in recent years, leading to

A.C. Varonides (✉)
Physics and EE Department, University of Scranton, Scranton, PA, USA
e-mail: varonides@scranton.edu

S. Logothetidis (ed.), *Nanostructured Materials and Their Applications*, NanoScience and Technology, DOI 10.1007/978-3-642-22227-6_5,

solar cells of efficiency levels well above 30% (Fraunhofer Institute's multi-gap solar cell at 40.8%, and NREL's device at 40.2% respectively). Successful alloys have demonstrated high performance, such as $In_xGa_{1-x}P$ alloys (x (%) of gallium phosphide and (1 − x) (%) of indium phosphide). Other successful candidates, in current use and perpetual cell design consideration, are the lattice-matched GaAs/AlGaAs and InP/GaAs pairs or AlAs/GaAs/GaAs triple layers and alloys, which are heavily used in both solar and the electronics industry. In this chapter, combinations of lattice-matched layers are considered in a current high-efficiency solar cell design. In spite the fabrication costs, these multilayered solar cells are here to stay: international collaborative research and development efforts are currently leading to high and very-high efficiency solar cells of tiny size, embedded in sophisticated Fresnel-optics tracking systems with great expectations (concentrated photovoltaics or CPV).

5.1 What is a Solar Cell?

A p-n junction is necessary for a solar cell to operate under illumination. Basically, solar photons of a specific range (either from the visible or the infrared) may be absorbed by semiconductor layers involved in the cell structure. The energy band of a semiconductor includes the valence and conduction bands, separated by a forbidden gap of energy. The latter is characteristic of the medium involved (e.g., for silicon, the gap energy is 1.12 and for germanium 0.67 eV respectively). The cell structure is fundamentally a p-n junction: given a semiconductor, there has to be a way to extract free carriers by means of illumination. Incident photons are supposed to be absorbed by the medium at energy values very near the gap energy of the medium. For free carriers to be collected as measurable external current, a specific design must exist: somehow, an electrostatic field that could sweep out the carriers from the region of their generation, before these carriers recombine (lost or return to the valence band). Non-zero fields can be formed via p- and n-regions in direct contact. Therefore, a typical bulk cell is implanted with two p and n regions in contact, thus forming a p-n junction. As p- and n- carriers form space charge regions across the junction, a depletion region is formed with non zero electric field which is maximum at the interface and decrease down to zero at the edges of the two regions. When a carrier finds itself in the depletion region, it eventually accelerates along or against the field (depending on its charge). The latter process is the key operation for all solid state devices: their basic function is based on the existence of one or more p-n junctions (optical devices are based on p-n junctions as the main regions where electrons and holes can essentially separate from each other to form photo-currents). Typically, in an illuminated p-n junction, photons are absorbed and electron-hole pairs are generated. These carriers eventually diffuse in opposite directions (separated by the existing electrostatic field at the junction), and within their respective diffusion lengths. Electrons at the

p-side slide down the junction potential and holes get to the opposite directions. Under open-circuit conditions, the voltage across the cell is given by the following formula:

$$V_{oc} = kT \ln\left(1 + \frac{I_L}{I_o}\right) \tag{5.1}$$

Where k is Boltzmann's constant, T(°K) is temperature, I_L is the light-generated current, and I_o is the p-n junction's reverse saturation current. On the other hand, when it comes to the experimental characterization of the cells, a quantity called internal quantum efficiency is useful: the number of excited electrons, for each absorbed photon.

5.2 Photo-Currents

Solar photons strike the surface of the cell at all wavelengths, from below the edge of the visible to near far infrared (IR). Just above the earth's atmosphere, the solar spectrum is similar to 6,000°K black body (AM0 conditions). At sea level, the atmospheric absorption modifies the solar irradiance ($\mathrm{mW/cm^2}$) to about $100\,\mathrm{mW/cm^2}$ (AM1.5 conditions). Photons of energy below the energy gap do not get absorbed by the material; photons with energies at the gap edge and above have a finite chance of being absorbed. Fundamentally, each photon will generate one hole-electron pair. This means that the number of photo-carriers is equal to the number of incident photons that are absorbed. Far from the junction, the electric fields are weak and carrier transport occurs by diffusion. In the n-region, holes diffuse to the junction, where they are collected and dragged by the field to the other side. Similarly, electrons in the p-region diffuse to the edge of the depletion region and get swept to the other side by means of the field in the depletion region. Fundamentally, solar cell modeling correlates incident solar photon flux F_{ph} (# $\mathrm{cm^{-2}\,s^1}$) with generation and recombination carrier rates in the interior of the device. Photo-generated concentrations of diffusing carriers are typically found (modeled) through the diffusion equation (under appropriate boundary conditions):

$$D_p \frac{d^2 p_n}{dx^2} - \frac{p_n - p_{no}}{\tau_p} + \alpha(1 - R) F_{ph} e^{-\alpha(x+d)} = 0 \tag{5.2}$$

Where p_n and p_{no} are carrier concentration after and before illumination (note excess carrier concentration is ($\delta p = p_n - p_{no}$), D_p is carrier diffusion coefficient, α is the material absorption coefficient, R is the reflection coefficient of the n-layer, and where x represents one-dimensional diffusion of carriers through the p-n

junction. Typical next step after solving for p_n or n_p is diffusion current evaluation via standard techniques and based on the following:

$$J_p = -qD_p \left(\frac{dp_n}{dx}\right)_{x=x(j)} \tag{5.3}$$

$$J_n = qD_p \left(\frac{dn_p}{dx}\right)_{x=x(j)} \tag{5.4}$$

Photon-collection efficiency is usually defined as:

$$\eta_{\text{col}} = \frac{J_p + J_n}{qF_{ph}} \tag{5.5}$$

Boundary conditions include continuity of carrier concentrations at the junction $x(j)$, and the dependence of the first derivative of carrier concentration on recombination velocity s_p, at the edge of the window layer as shown in the figure below:

$$\left(\frac{dp}{dx}\right)_{x=-d} = \frac{s_p}{D_p}(p(-d) - p_{no}) \tag{5.6}$$

The figure below indicates a generally accepted modeling geometry for a p-n junction solar cell.

5.3 Solution of the Diffusion Equation: n-Region

Minority holes are expected to be generated in the window layer (x from –d to 0)

$$p_n(x) - p_{no} = A\cosh(x/L_p) + B\sinh(x/L_n) - \frac{\alpha F_{ph}(1-R)(L_p^2/D_p)}{(\alpha L_p)^2 - 1} e^{-\alpha(x+d)} \tag{5.7}$$

Based on the boundary conditions as mentioned above:

$$A = \frac{\alpha F_{ph}(1-R)(L_p^2/D_p)}{(\alpha L_p)^2 - 1} e^{-\alpha d} \tag{5.8}$$

$$B = \frac{\alpha F_{ph}(1-R)(L_p^2/D_p)}{(\alpha L_p)^2 - 1} \tanh(d/L_p) + \frac{\alpha^3 F_{ph}(1-R)(L_p^3/D_p)}{\cosh(d/L_p)(\alpha^2 L_p^2 - 1)} + \frac{s_p L_p}{D_p} \frac{[p(-d) - p_{no}]}{\cosh(d/L_p)} \tag{5.9}$$

Substitution of A, B constants provides a complete solution for minority holes in the n-region of the cell. Total electric current J_p coming from the n-region is naturally following from the diffusion current formula (see above). Specifically, maximum hole-current from the n-region is:

$$J(x=0) = -qD_p K \times \left[\frac{1}{L_p}\left[\tanh\left(\frac{d}{L_p}\right) + \frac{\alpha L_p}{\cosh(d/L_p)} + \frac{s_p L_p}{D_{pK}} \times \frac{p(-d) - p_{no}}{\cosh(d/L_p)}\right] + \alpha e^{-\alpha d}\right] \tag{5.10}$$

Where

$$K = \frac{\alpha F_{ph}(1-R)(L_p^2/D_p)}{(\alpha L_p)^2 - 1} \tag{5.11}$$

5.4 Solution of the Diffusion Equation: P-Region

Minority electrons develop in the p-region under the following boundary conditions:

$$[n_p - n_{po}]_{x=W} = 0 \tag{5.12}$$

And

$$-D_n\left(\frac{dn}{dx}\right)_{x=L+W} = s_n(n_p - n_{po}) \tag{5.13}$$

The diffusion equation reads as follows:

$$D_n\frac{d^2 n_p}{dx^2} - \frac{n_p - n_{po}}{\tau_p} + \alpha(1-R)F_{ph}e^{-\alpha(x+d)} = 0 \tag{5.14}$$

Solution of (5.14) is of similar kind with (5.7) along with boundary conditions (5.13):

$$n - n_{po} = A\cosh(x/L_n) + B\sinh(x/L_n) - \frac{\alpha F_{ph}(1-R)(L_n^2/D_n)}{(\alpha L_n)^2 - 1}e^{\alpha(x+d)} \tag{5.15}$$

With A, as in (5.8):

$$A = \frac{\alpha F_{ph}(1-R)(L_n^2/D_n)}{(\alpha L_n)^2 - 1}e^{-\alpha d} \tag{5.16}$$

And B as in (5.9):

$$B = -\frac{s_n L_n}{D_n} \times \frac{n_p({}_nL + w) - n_{po}}{} \times \cosh\left(\frac{L_n + w}{L_n}\right) - \frac{\alpha F_{ph}(1-R)(L_n^2/D_n)}{(aL_n)^2 - 1}$$
$$\times \tanh\left(\frac{L_n + w}{L_n}\right) - \frac{\alpha^2 F_{ph}(1-R)(L_n^3/D_n)}{((\alpha L_n)^2 - 1)\cosh(\frac{L_n+w}{L_n})} \times \exp(-(d + L + w)) \tag{5.17}$$

5.5 Total Electron and Hole Currents

Electron current:

$$J_n = \frac{qD_n}{L_n} \times \frac{\alpha F_{ph}(1-R)\tau_n}{(\alpha L_n)^2 - 1}$$
$$\times \left\langle \sinh(W/L_n) - \left[\frac{s_n L_n}{D_n} \times \frac{n_p(w+L) - n_{po}}{\cosh\left(\frac{L+w}{L_n}\right)} \times \frac{(\alpha L_n)^2 - 1}{\alpha F_{ph}(1-R)\tau_n} \right.\right.$$
$$\left.\left. + \tanh\left(\frac{W}{L_n}\right) + \frac{e^{-\alpha(d+L+W)}}{\cosh\left(1 + \frac{W}{L_n}\right)} \right] \times \cosh\left(\frac{W}{L_n}\right) + \alpha L_n e^{-\alpha(W+d)} \right\rangle \tag{5.18}$$

Where $\tau_n = L_n^2/D_n$
Hole-current:

$$J_p = -\frac{qD_p}{L_p} \frac{\alpha F_{ph}(1-R)\tau_p}{(\alpha L_n)^2 - 1}$$
$$\times \left\{ \tanh\left(\frac{d}{L_p}\right) + \frac{\alpha L_p}{\cosh\left(\frac{d}{L_p}\right)} \right.$$
$$\left. + \frac{s_p L_p}{D_p} \frac{(\alpha L_p)^2 - 1}{\alpha F_{ph}(1-R)\tau_p} \frac{p(-d) - p_{no}}{\cosh\left(\frac{d}{L_p}\right)} + \alpha L_p e^{-\alpha d} \right\} \tag{5.19}$$

5.6 P-I-N Geometries of Solar Cells

P-n junctions with long intrinsic (less impurity scattering) regions provide a wide range for photo-electrons to escape the depletion region (before recombination) and to be collected at the load. This advantage combined with the idea of using a heterojunction p-n interface instead of a bulk counterpart has led to many exciting cell designs. In the figure below, one may observe the discrete energy levels due to two semiconductors of different band gaps.

Candidate materials in such cases could be AlAs and GaAs for wide and narrow band gaps, respectively. Coupled with the idea of capturing a wider range of photons, the intrinsic region can be replaced by a sequence of layers with different band gaps (a superlattice) as shown in Fig. 5.1, below:

Photo-Carriers are trapped in quantum wells, and subsequently (a) tunnel through layers and/or (b) escape thermionically from the quantum wells. Initial selection of width can lead to specific eigen-energy level formation, as shown on the above. The ground and second (at the most) states provide carrier populations near 10^{12} cm^{-2}. If the second energy level is near the edge of the wells, it will eventually lead to smooth electron hopping, while tunneling might dominate at the ground level. If the thickness of the wells is selected such that only one solution exists in the wells, then carriers either escape thermally or tunnel through thin barriers. Thermal escape however will be dominant when thick barriers are selected (which is the case of Fig. 5.2).

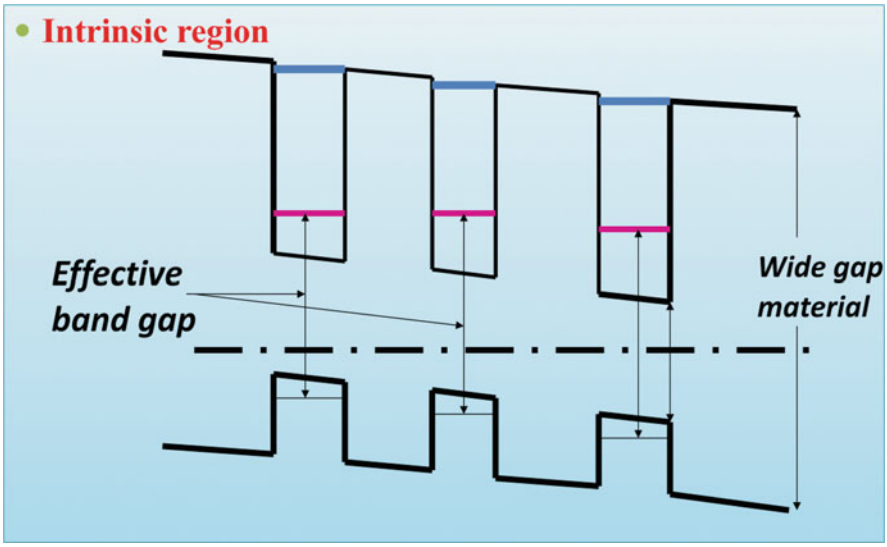

Fig. 5.1 Detail from a superlattice structure (typically GaAs/alloy and GaAs/Ge (as proposed in this study). The dashed line represents the Fermi level at thermal equilibrium. The optical gap can be tuned to desired energy values

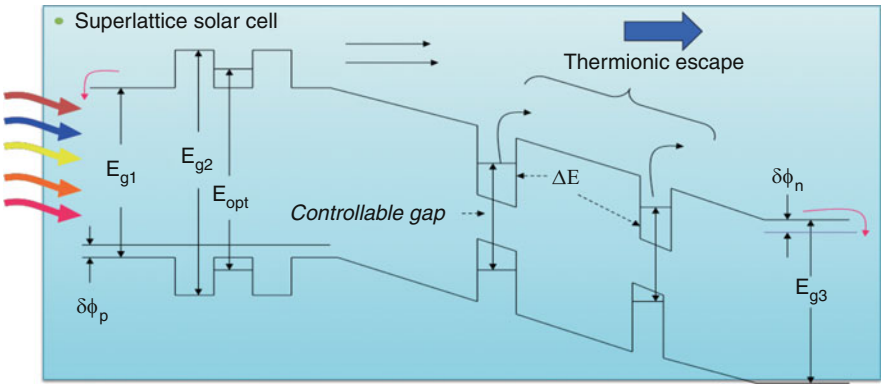

Fig. 5.2 An improved solar cell design with more than two layers. Note the existence of quantum traps in the intrinsic region, and the quantum well in the p-region (far left)

As seen from Fig. 5.2, a number of issues are of concern:

1. Note the double-barrier (DB) structure in the p-region: it may be a set of alternate GaAs/AlAs/GaAs layers, where the DB structure will provide excess photo-carriers at desired (long) solar wavelengths.
2. Note the proposed intrinsic region: a sequence of multiple quantum wells (MQWs) is proposed, so that desired incident solar wavelengths can be absorbed as well (especially in the 1 eV range).
3. The last layer is proposed to be either GaAs or Ge (0.66 eV hence long wavelength absorption).
4. Visible light absorption made possible via the AlAs layers (far left).
5. Tunneling possibility through energy eigen-states in the quantum wells: note the double well (DW) structure in Fig. 5.2, where transmission is at its maximum at peak values of the transmission coefficient. Selecting barrier thickness well thickness, may lead to peak current values from the AlAs layer down the bulk GaAs region. Note also that DW geometries may play a key role in multijunction solar cells: they provide a series connection layer to lower portions of the device (MJ cells and cells in tandem).

Based on the above points, combination of tunneling and thermionic currents may lead to wide solar spectrum absorption, depending on the design adopted. Note also the tunnel-diode structure on the left side of the device, with sequential or resonant tunneling possibilities.

5.7 A Proposed Device

Very recently, we have proposed an undoped GaAs-Ge MQW in a standard p-i-n design, namely, p-intrinsic (MQW)-n geometry that includes lattice-matched GaAs and Ge layers in the intrinsic region of the PV device. This formation offers the

advantage at 1 eV absorption in the III–V realm, without compromises in device transport properties, such as mobility or conductivity. GaAs-based layers ensure (a) high mobility and absorption values (via GaAs and *thin* Ge layers) and (b) fine-tuning of the *optical gap* with solar photon wavelength.

The proposed design is a part of a more complex structure that includes the top and bottom cells in tandem. Calculations regarding both parts of the device are showing results as follows: (a) Top sub-cell (AlAs-AlGaAs-GaAs): in excess of 21% (Varonides et al., WREC 10, Glasgow 2008) conversion efficiency predicted for a 1 cm^2 cross section lattice-matched AlAs/AlGaAs/GaAs unit in the visible (AM1.5, one sun). Modeling is based on bulk layer calculations for n^+ (window)–n–p triple junction solar cell. As second choice for a top layer, we include a 30% metamorphic triple-junction InP-GaAs-GaAs solar cell. (b) Bottom cell: eigen-energy fine tuning calculations lead to carrier confinement and subsequent carrier escape with thermionic emission and nearest neighbor hopping (NNH) conduction from site to site. Carrier escape from the quantum wells is thought to be a thermionic process, along with recombination losses. Incident IR photons are expected to be absorbed in the MQW area of the structure, while recombination losses are taken into account. Projected excess carriers (electrons) are of the order of 10^{12}–10^{13} cm^{-2} per ground eigen-state. Thermionic current density values are then projected in the order of 30 mA/cm^2 and open-circuit voltage values above 1 V, at one sun. Overall (composite device) collection efficiency values are initially projected well in excess of 40%, which is a key threshold target for current high efficiency PV. Photon shadowing issues can eventually be overcome with appropriate optical design (for instance, cell placed at the focal plane of a parabolic or concave mirror, where both sides are illuminated simultaneously).

Total current density is dominated by the lowest of the two sub-cell currents, and open-circuit voltage values are the sum of the two sub-cell V_{oc} values. Total current from the bottom cell is the sum of thermionic and nearest neighbor hopping currents (NNH, Varonides, and Spalletta). Preliminary results reach estimates of efficiencies from each of the two (lattice-matched) sub-cells in excess of 21% per cell (predicted synergy of the two sub-cells in excess of 40%). Loss mechanisms at interfaces and quantum wells and their role in overall efficiency determination will also be included.

Advantages of the design are:

1. Solar spectrum matching in both visible and IR ranges through layer band gap-matching selection.
2. Lattice-matching and hence less carrier scattering (3) improved carrier transport due to GaAs (no mobility problems as in III-N-V hetero-solar cells). It is conceivable that even the 50% target of conversion efficiency will be reached with such a design.
3. No tunnel junctions (TJ) needed (1) the p-layer of the top cell is the same p-layer of the p-i-n superlattice, with no TJ need. Instead, the superlattice itself is a set of successive tunnel junctions (quantum well and barrier interfaces).

Heterostructure and (most recently) multijunction solar devices exhibit better performance in transport properties, when compared to bulk solar cells: especially in quantum well devices, photo-excitation causes carrier accumulation in discrete energy levels, with subsequent escape to the conduction band (minus recombination losses) via standard mechanisms such as tunneling, thermal escape or NNH conduction. Full spectrum absorption and triple junction solar cells have become key factors for high efficieny collection in PV structures of various geometries. Most recently, successful PV device designs have shown high efficiency values well above 30%, and efficiency levels in excess of 40% have been reached by means of triple junction metamorphic solar cells and under high sun concentration (good candidate for concentrated PV or CPV). Multijunction solar cells offer a great advantage over their bulk counterparts: by incorporating lattice-matched alloys, one may succeed in designing a device with more than one energy gaps thus increasing the number of absorbed solar photons. During the last decade, various groups have modeled and developed *multijunction* solar cells in order to increase overall collection efficiencies. Emphasis has been given in two types of PV devices (a) lattice-matched solar cells and (b) metamorphic (lattice-mismatched) solar cells. In particular, III–V multijunction solar cells have shown the greatest progress in overall efficiency.

5.8 The Concept

The broader impact of this project is a new design proposal for high efficiency solar cells. The target is to exceed 45% collection and thus to open the way to very efficient PV. It is more than clear that, once such a cell is realized, the field of concentration photovoltaics (CPV) will benefit greatly: solar cells with (a) record high efficiency values, (b) under several hundred suns (typically Fresnel optics at 500+ suns), and (c) small in size (low area hence less material) is already attracting interest for mass production in many places in the world. In recent years, it has been proposed by us a new design for a high efficiency and lattice-matched solar cell (HESC), where both visible and IR portions of the solar spectrum are absorbed according to the structure's geometric material arrangement: simultaneous absorption of both short and long wavelengths. In this on-going research enterprise the synergy, between a highly efficient triple junction cell and a highly efficient superlattice or a multi-quantum well region, is presented as a new and innovative way for further efficiency increase. It is well established by now, that triple junction solar cells are exceeding the upper threshold of collection efficiency to ever higher levels, namely above 38% with latest threshold at 40.8%. Currently, we are targeting a cell structure that will operate above the 40% threshold, with ultimate target the efficiency at or near 50%. Our proposal is based on a p-i-n bulk device model with three distinct areas, two of which are complete PV-heterostructures on their own, in other words these two regions could *stand alone* as two independent solar cell structures with quite acceptable performance (of the order of 21% and more as it has been demonstrated by our group recently). The power output of the PV composite

device is a function of the individual power outputs from each sub-cell in the PV unit. A general formula of the *composite efficiency* will be discussed later on. Our group has already modeled a 21% triple junction AlAs/AlGaAs/GaAs solar cell. In parallel to that, our group has found more efficient options with various material combinations at higher yields. This task is in unison with other groups' work in the high efficiency solar cells. On the other hand, triple junction solar cells seem to lead the way to high efficiency PV especially in the area of CPV, where small cell area and therefore less material (hence lower material costs) may lead to high PV performance. The latter are triple junctions of lattice-matched and non-lattice matched III–V heterostructures with two tunnel junctions between the layers.

5.9 Current Research Objectives: A Proposed Guideline

1. Fully develop a theoretical model of PV composite PV devices by first principle calculations and computations based on realistic device parameters; propose a composite PV structure with two major cells: a triple junction and multi-layer tuned cell, with the prospect of high efficiency near 50%. Modeling tools include several established math software packages.
2. Seek for a composite PV device that combines properties of direct-gap crystalline semiconductors and absorption in the entire spectrum (as shown in Fig. 5.3 below), mainly in the visible and in the IR (NIR/IR) wavelength ranges, and which is configured as a two-part solar cell: a top triple junction and a multi-layer p-i-n bottom unit tailored to IR wavelengths. The solar spectrum (a 6,000 degree black body, shown in Fig. 5.4) offers the option of finding suitable band gaps for highest absorption. Material selection shows a blue shift in the absorption via wide gap materials as shown. On the other hand, low gap materials offer wavelength matching in the IR range.
3. Exploit the advantages of quantum wells grown on n-type or low-doped substrates. Seek for the synergy between a high efficiency triple junction of

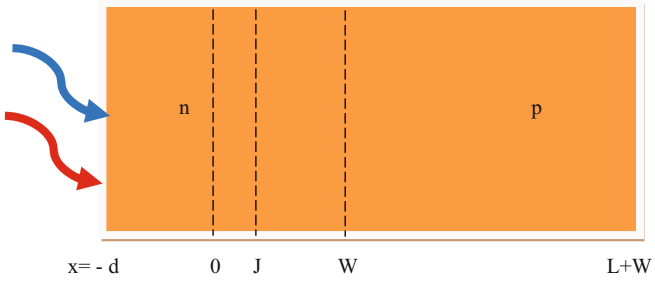

Fig. 5.3 Typical modeling geometry of a solar cell: w is the depletion width, J is the exact interface, L is the width of the p-region and d is the n-region (window layer), and w is the depletion width

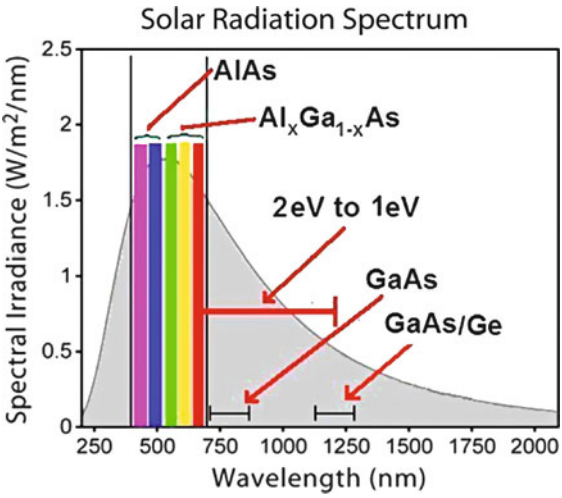

Fig. 5.4 Regions of the solar spectrum covered by the superlattice cell and the top cell (visible). The superlattice can be finely tuned at ~1 eV (via optical gap or energy distance between lowest electron and hole energy levels in quantum wells). Note the range for GaAs-Ge region of absorption

our own design and a MQW/superlattice structure (where quantum size effects are dominant). Superlattice structures in both cases mentioned above are at the designer's disposal, in the sense that appropriate quantum well geometries may lead to desired solar photons absorption.

4. Enhance cell performance by replacing the intrinsic region by a *finely-tuned lattice-matched MQW layer* via a wide gap – low gap sequence, but in such a way that *specific* range of wavelengths will have a chance to be absorbed. The latter region will be treated as a quantum trap of photo-generated electrons and holes. Photo-carriers trapped in quantum wells (medium with lower gap) may (a) recombine (b) escape from quantum wells into the conduction band of the wide gap medium, and/or (c) tunnel through thin barriers (if so desired). Thermionic emission, hopping conduction, and tunneling are dominant mechanisms of photo-carrier transport in heterostructures (against losses due to recombination processes). In the type of device in mind, and especially in its intrinsic region quantum wells, incident solar photons typically generate 10^{12}–10^{13} net photo-excited carriers per unit area (cm^2), after recombination effects have been taken into account. This population is expected to migrate to the conduction band assisted by the escape mechanisms named above and the built-in electrostatic field in the p-i-n region. It is also worth noting that the proposed design provides degrees of freedom in the sense that various lattice-matched material combinations (e.g., GaAs and alloys) may be considered for cell design, and at specific wavelength ranges.

5. Grow an **AlAs/AlGaAs/GaAs** lattice-matched n-n-p hetero-cell on top of a p-i-n quantum well based and lattice-matched cell. The **AlAs/AlGaAs/GaAs** option can reach collection efficiencies above 21%, if considered as a stand-alone solar cell. In addition, recent modeling of a triple junction **InP-GaAs-GaAs** cell, has shown 30% efficiency (1 cm^2 cell/one sun/1.5 AM conditions (Varonides, Spalletta 34th IEEE PVSC, June 7–12, 2009, Philadelphia). It is clear that an obvious advantage would be imminent if such a layer could be grown at the top of a p/i/n solar cell: the resulting proposed PV device includes two sub-cells in one. The proposed complete structures are: $\mathbf{n^+}$**-AlAs/n-AlGaAs/p-GaAs/i/(GaAs/Ge)$_{MQW}$/n-(Ge)** and $\mathbf{n^+}$**-InP/n-GaAs/p-GaAs)/i/(GaAs/Ge)$_{MQW}$/n-(Ge)**
6. Solve for thermionic currents in the intrinsic region; solar photons generate electron and hole pairs (EHP) when incident on a semiconductor layer. Photo-excited carriers may be trapped (confined) in quantum, wells and may either recombine or sustain a population in the eigen-energy levels. Existence of Ge-quantum wells serves this purpose: to confine a certain population of photo-excited electrons in the conduction band, out of which, a percentage is expected to escape to the conduction band of the surrounding material (GaAs). Given that electrons exhibit superior mobility values in un-doped GaAs, it is conceivable to expect improved transport properties in this GaAs-dominated PV device, over its III-N-V counterparts. Solving for thermal currents means (a) deriving an explicit expression of excess electrons $\delta n(x)$ per unit area (in any quantum well), (b) evaluating thermal currents out of each trap, (c) including recombination effects (mainly Auger and radiation recombination), and (d) solving the diffusion equation. The latter (diffusion of photo-electrons in the conduction band) involves a straightforward analytic method for solving the diffusion equation: by this method one is able to analytically predict carrier concentration in quantum wells (anywhere in the intrinsic region) and predict thermionic escape current density values, based on the excess carrier concentration $\delta n(x)$ (Varonides, Sze).
7. Solve for hopping conduction in the MQW region. NNH between quantum wells will be performed. NNH currents are non-zero in the intrinsic region. Carriers are expected to hop from energy level to neighboring energy levels (Ge-Ge sites). Work so far has shown that hopping currents (Varonides, Spalletta) are:

   (a) non-zero from site to site in the intrinsic region
   (b) strong functions of the Fermi level position relative to the band gaps in the intrinsic region
   (c) more specifically, we have concluded that hopping currents are related to Fermi level splitting at any two adjacent sites
   (d) depending on device geometry (quantum well width and barrier)
   (e) depending on temperature
   (f) conduction band discontinuity
   (g) density of states in the quantum wells.

8. Fine-tune at specific wavelengths in the IR region. Current research on crystalline solar cells focuses on a maximization of incident radiation absorption at all possible wavelength ranges, namely, from the visible to the near infrared (NIR). Currently, III-N-V's are being promoted for NIR absorption, but not without drawbacks: *low mobility* issues in (III-N-V) solar cells cause serious weakening of the advantages over NIR absorption. To overcome this problem we are proposing a superlattice structure in a standard p-i-n PV device, where the intrinsic region is replaced by a sequence of lattice-matched GaAs-Ge layers with pre-selected Ge (low gap) thickness chosen in such a way that overall optical gap values occur at or near 1 eV (Fig. 5.4). Quantum wells in the intrinsic region of the bottom sub-cell provide photo-excited carriers via the eigen-energy levels. Incident solar photons at long wavelengths can be collected (absorbed) by semiconducting layers with band gaps equal to the photons' energy. Quantum wells fit perfectly in the matter, causing increase of the band gap of the semiconductor (optical gap). Optical gap values can be tailored according to the incident photonic wavelength: eigen-energy levels in quantum wells are strong functions of well width (at any semiconductor interface there is a conduction band and a valence band discontinuity (ΔE_c and ΔE_v respectively)); the depth of the quantum well is equal to ΔE_c (for electrons). Thus, absorption can be finely tuned by selecting a priori the well width so that optical energy values are at desired wavelengths dictated by incident solar photons. So, first principle modeling and computations of Ge-quantum wells neighbored by GaAs layers (barriers) will be needed. As it has been realized in the wider literature, absorption at one electron-volt is desired (wavelengths near 1.24 μm). Absorption in the area of 1 eV is easily achievable by appropriate well width selection; this is the innovative idea: to (a priori) select optical gap energy values near 1 eV for IR absorption. An obvious advantage of the superlattice or MQW-based fine tuning is that different materials can be used (the more lattice-matched the better) for different optical gap-based absorption. Note also that eigen-energy levels in quantum wells (or quantum dots) may serve as second order absorbers (For instance, in a given QW arrangement, a second a hole-electron optical gap may correspond to 1.33 eV (very close to InP- band gap!), which translates to 0.932 μm absorption and so on (Fig. 5.5).
9. Select geometry of the quantum wells such that two (at the most) energy levels in the quantum wells are to be formed, namely, the ground state of electron-hole pairs at 1 eV, and the second state at the very *edge* of the GaAs layer conduction band this event has been shown to act in favor of *nearest neighboring hopping electrons*from site to site (QW). Thus a threefold advantage of the superlattice/MQW region is that (1) carriers are trapped and thermally escape to the conduction band, (2) NNH conduction becomes a second conduction mechanism, and (3) band gaps of other materials may be represented via energy levels in quantum wells.

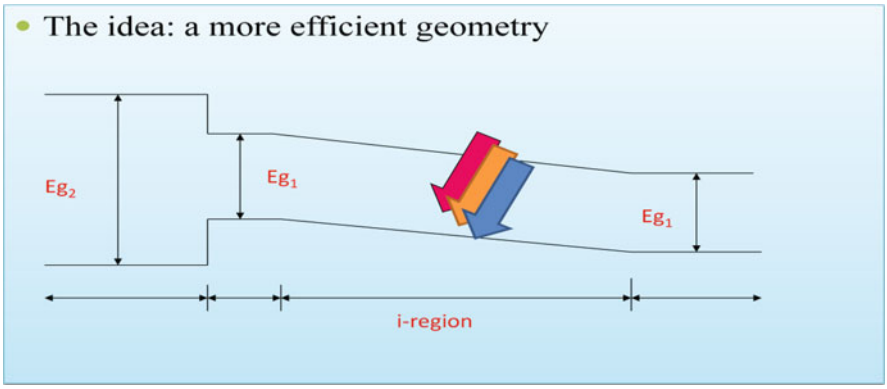

Fig. 5.5 A heterojunction p-i-n solar cell; high and low gaps serve for high and low energy or short and long wavelength photon absorption (visible and infrared respectively)

10. Calculate total efficiency by realizing the fact that two solar cells will eventually absorb input power according to their capability of photon absorption at the right portions of the solar spectrum. If P_{in} is the total input power, n_1, n_2 are the individual efficiency values of the two sub-cells involved in the device design, then the power output P_{o} is found from the following formula:

$$P_{\text{o}} = n_1 P_{\text{in}} + n_2(P_{\text{in}} - P_{\text{o1}}) = (n_1 + n_2)P_{\text{in}} - n_1 n_2 P_{\text{in}}$$

Total efficiency for two sub-cell multijunction PV-device is:

$$n = n_1 + n_2 - n_1 n_2$$

(where) $\eta_1 = \frac{P_{\text{o1}}}{P_{in}}$.

In conclusion, the total current from the intrinsic region will be the sum of the thermionic and the NNH current components (minus recombination losses). Subsequent well width selection may lead to further refinement of solar photon absorption. Near IR and IR portions of the solar spectrum can be covered by suitable width selections, with equal amount of modeling effort (from the point of view of computations, it is a mere change of parameters for slightly different optical gaps). It is also interesting to note at this point that quantum well width could be modeled as a random variable, leading to a random distribution of optical gap values (as function of well width) and hence a smeared distribution of optical gap values and absorbed photon wavelengths, for the benefit of the PV device. The latter ensures IR photon absorption in the neighborhood of 1 eV and beyond (depending on the energy distance between eigen-energy levels in the quantum well), along with parallel minimization of electron capture, through NNH. In addition, the superiority of transport properties of the proposed quantum-PV device should be noted compared to its III-N-V "high" efficiency counterpart: our proposed MQW

solar cell is mainly a GaAs device perturbed by thin Ge layers, and therefore this region exhibits much higher electron mobility. In the absence of tunneling (thick potential barriers) total currents are in essence the sum of thermionic and hopping current components, due to free electrons in the GaAs conduction band, assisted by the overall electrostatic field in the intrinsic region. The energy band diagram of the complete device is shown in Figs. 5.2 and 5.4: the existence of a window with "Anti-Reflecting-Coating" and surface texturing is included to minimize reflections, while shown are the top and bottom sub-cells. The goal in the top cell is either to retain visible absorption (AlAs/(Al) GaAs/GaAs at 21%) or to include a highly efficient triple junction cell (in this proposal, our own choice (InP/GaAs/GaAs at 30% efficiency). Wide-gap window materials (like AlAs, $Al_xGa_{1-x}As$) provide absorption from the blue to the red portion of the spectrum; the p-i-n part of the composite PV device covers the NIR and IR portion.

Figure 5.6 depicts a structure with various layers shown. Note also that in such a structure, there is no need for tunnel junctions for the carriers to migrate from region to region. Instead, excess photo-carriers from the top-cell will migrate to the p-type GaAs layer and they will drift in the intrinsic region assisted by the electrostatic field. Escaping photo-carriers from the intrinsic region will diffuse to the end of the device. Lack of tunnel junctions in the device is of fundamental importance over currently highly efficient multijunction solar cells. The mere fact that tunnel junctions are absent indicates:

1. less material to grow
2. less complexity in the structure overall
3. reduced scattering of drifting and diffusing carriers
4. reduced carrier trapping and recombination (carriers in MQW region separate from their corresponding holes as being away from the quantum wells)

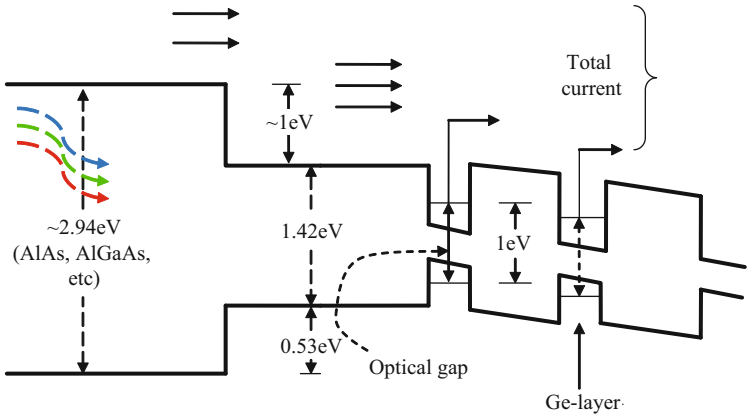

Fig. 5.6 Quantum PV structure: Bird's eye view of the device design proposed: shown are (**a**) different gap layers of the top cell, (**b**) GaAs-Ge layers in the intrinsic region, (**c**) optical gap at 1 eV, and (**d**) total conduction band free electrons due to thermionic escape and hopping conduction

5. faster growth conditions attainable
6. less fabrication costs.

Top cell design ensures visible wavelength absorption (via AlAs-AlGaAs-GaAs double junction cell) and the bottom cell provides absorption in the IR or near 1 eV (depending on the eigen-energy tuning in via the quantum wells).

5.10 To Probe Further

Cell structures of the type depicted above are promising state of the art PV devices with high currents (in excess of 30 mA/cm^2 and increased open-circuit voltage (OC) values: near one volt per subcell under one sun). The latter notion related to the fact that the two sub-cells are considered to be connected in series, where the OC voltages are in essence in excess of two volts. This would lead to cumulative collection efficiency values well in excess over 40%; for instance: for a very realistic fill factor (FF) near 80%, for final matched currents in the neighborhood of 25 mA/cm^2 *(a conservative value for such high-current structures*), and for OC voltage near 2 Volts, the overall one-sun efficiency of the cell (as the one shown by Fig. 5.7) would exceed the 40% current threshold! Optimization of matching currents between the sub-cells needs to be explored further; superlattice based cells

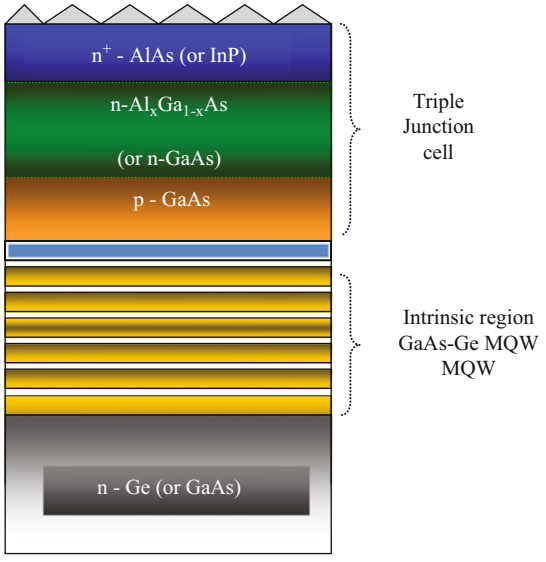

Fig. 5.7 Proposed PV-structure with two sub-cells: bulk top lattice-matched structure for the visible, and bottom cell structure for NIR, IR photons. The region between the two cells could be a tunnel junction to ensure current matching between the two cells

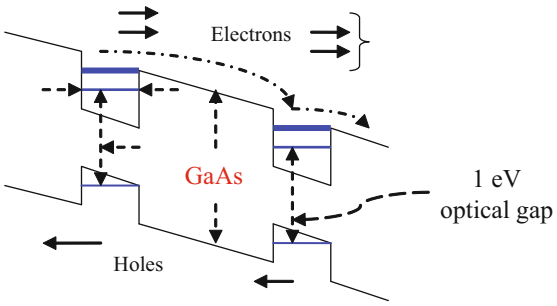

Fig. 5.8 Fine tuning at specific wavelengths can be achieved through quantum size effects in the quantum traps of the intrinsic region. Electrons' thermionic escape and NNH conduction are shown at the conduction band. Note the eigen-energy levels in Q W's: by selecting the Ge-layer width, second order levels can reach the conduction band edge of GaAs

are known to carry high current and coexistence of such layers in a series connected fashion, may lead to substantial voltage increase and hence to higher than 40% efficiencies (Fig. 5.8).

References

1. M. Yamaguchi, Sol. Energy Mater. Sol. Cells **90**, 3068–3077 (2006)
2. M. Yamaguchi et al., Sol Energy **82**, 173 (2008)
3. R.R. King et al., APL **90**, 183516 (2007)
4. J.F. Geisz, S. Kurz, M.W. Wanlass, J.S. Ward, A. Duda, D.J. Friedman, J.M. Olson, W.E. McMahon, T.E. Moriarty, and J.T. Kiehl, Appl. Phys. Lett. **91**, 023502 (2007)
5. T. Kirchartz, U.w.e. Rau, et al., Appl. Phys Lett. **92**, 123502 (2008)
6. T. Mei, J. Appl. Phys. **102**, 053708 (2007)
7. G.F.X. Strobl, T. Bergunde, et al., in *4th World Conference on Photovoltaic Energy Conversion*, Hawaii, 8–12 May 2006
8. A.C. Varonides, R.A. Spalletta, Phys. Stat. Sol. **5**, (2) 441 (2008)
9. G.F.X. Strobl et al., in *Proceedings of the 7th European Space Power Conference*, 9–Italy, 13 May 2005
10. H.L. Cotal, R.R. King et al., 28th IEEE Photovoltaic Specialists Conference, p. 1316 (2000)
11. T. Kieliba, S.W. Riepe Warta, J. Appl. Phys. **100**, 093708 (2006)
12. J.F. Geisz, D.J. Friedman, Semicond. Sci. Technol. **17**, 789 (2002)
13. W. Hant, IEEE Trans. Electron Devices **26**, (10) 1573 (1979)
14. A.C. Varonides, Thin Solid Films **89**, 511–512 (2006)
15. A.C. Varonides, Phys. E **14**, 142 (2002)
16. A.C. Varonides, R.A. Spalletta, W.A. Berger, in *European Materials Society, Spring Meeting 2005, Palais des Congrès,*Strasbourg, France, May 28–June 1, 2007
17. E. Istrate, E.H. Sargent, Rev. Mod. Phys. **78**, 455 (2006)
18. H.E. Runda et al., Nanoscale Res. Lett. **1**, 99 (2006)
19. L. Lazzarini et al., Micron **31**, 217 (2000)
20. M. Razeghi, J. AP **23**, 141 (2003)
21. H.W. Li, B.E. Kardynal, et al., Appl. Phys. Lett. **93**, 153503 (2008)

22. S.M. Sze, *Physics of Semiconductors* (Wiley and Sons, NY, 1981)
23. A.C. Varonides, Thin Solid Films **511–512**, 89–92 (2006)
24. A.C. Varonides, in *Proceedings of the 3rd Workshop on Nano-sciences & Nanotechnologies*, (Aristotle University of Thessaloniki, Greece, 2006), p. 46
25. A.C. Varonides, in *Thin Film and Nano-structured Materials for Photovoltaics, Reprinted from Thin Films*, ed. by A. Slaui, A. Jager Waldau, J. Poortmans, V. Brabec, E-MRS 2006, EMRS Proceedings 180, (Elsevier), Nice, France, p. 89
26. A.C. Varonides, in Hopping conduction III-N-V hetero-junctions, *Presented at the European Materials Society*, Strasbourg, France, May 31 2007
27. A.C. Varonides, R.A. Spalletta, W.A. Berger, in *European Materials Society, Spring Meeting 2005, Palais des Congrès,*Strasbourg, France, May 28–June 1 2007
28. A.C. Varonides, R.A. Spalletta, W.A. Berger, in *E-MRS, European Materials Society, Spring Meeting 2005, Palais des Congrès,*Strasbourg, France, May 28–June 1 2007
29. A.C. Varonides, R.A. Spalletta, Phys. Status Solidi (c) **5**, (2) 441–444 (2008)
30. A.C. Varonides, R.A. Spalletta, W.A. Berger, in *Proceedings of the World Renewable Energy Congress (WREC) X and Exhibition*, 19–25 July 2008, Scottish Exhibition & Conference Centre, Glasgow, Scotland, UK